

# Dynamics of Coalescence of Plugs with a Hydrophilic Wetting Layer Induced by Flow in a Microfluidic Chemistode

Ying Liu<sup>†,‡</sup> and Rustem F. Ismagilov<sup>\*,†</sup>

Department of Chemistry and Institute for Biophysical Dynamics, The University of Chicago, 929 East 57th Street, Chicago, Illinois 60637

Received October 22, 2008. Revised Manuscript Received December 9, 2008

This manuscript analyzes the dynamics of coalescence of an incoming aqueous plug with a wetting layer above a hydrophilic surface in the chemistode. The chemistode is a recently described (Chen, D.; Du, W.; Liu, Y.; Liu, W.; Kuznetsov, A.; Mendez, F. E.; Philipson, L. H.; Ismagilov, R. F. *Proc. Natl. Acad. Sci. U.S.A.* **2008**, *105*, 16843–16848) microfluidic analogue of an electrode, but operating at the chemical rather than electrical level, developed with the aim of capturing local stimulus-response processes in chemistry and biology. The chemistode consists of open-ended V-shaped microfluidic channels that can be brought into contact with a chemical or biological hydrophilic substrate. The chemistode relies on multiphase aqueous/fluorous flow and uses plugs to achieve high temporal resolution of stimulation and sampling. Coalescence of the incoming plugs, containing the stimuli, with the liquid in the wetting layer is required for chemical exchange to take place in the chemistode. Here, we investigate the system with triethyleneglycol mono[1H,1H-perfluorooctyl]ether R/OEG as the surfactant. This surfactant was necessary to prevent nonspecific absorption of proteins to the aqueous fluororous interface and to ensure biocompatibility of the system, but too much surfactant increased the barrier for coalescence. In this system, coalescence was controlled by the capillary number. At a higher value of the capillary number, coalescence took more time, and deformation of the interface of the incoming plug and the wetting layer was more significant. Above a critical capillary number, coalescence did not occur between the incoming plug and the wetting layer. The critical capillary number was an increasing function of surface tension but was independent of viscosity ratio. Coalescence was surprisingly reproducible, presumably because film rupture during coalescence was reliably initiated at the hydrophilic substrate. These results are useful in rational operation of the chemistode and also provide an experimental description of deformation, film drainage, and coalescence of surfactant-coated droplets in an external flow field.

## Introduction

This paper describes the coalescence dynamics of an incoming aqueous plug with a wetting layer on a hydrophilic substrate within a microfluidic chemistode. The chemistode was recently developed and investigated to deliver pulses of chemical stimuli and to capture released pulses of molecular signals with high temporal resolution and efficiency.<sup>1</sup> The chemistode was designed with open-ended V-shaped channels, and it can be applied to a biological or chemical surface for stimulation and sampling (Figure 1). At the open end of the chemistode, the angle between the inlet and outlet tubing is 90°. The chemistode uses two-phase aqueous/fluorous plug flow to transport solutions without dispersion and losses to walls of channels. An array of aqueous plugs is delivered to a hydrophilic surface from the inlet tubing. The hydrophilic surface always holds a wetting layer above it. The incoming plugs coalesce, and mass transfer occurs between the incoming plug and the aqueous solution of the wetting layer, while the fluorocarbon carrier fluid remains in contact with the wall of the chemistode, provided that the capillary number is below a critical value. Finally, the plugs are re-formed in the outlet tubing.

Recent advances in microfluidics using multiphase flow as discrete nanoreactors for the reliable transport and reaction of

solutions<sup>2</sup> have attracted interest for studying controlled coalescence of droplets. This controlled coalescence, or fusion, can be electrocoalescence,<sup>3–5</sup> optical coalescence,<sup>6</sup> coalescence induced with microfluidic geometry,<sup>7–10</sup> surface-induced coalescence,<sup>11</sup> or coalescence induced with a flow field.<sup>12</sup> During these coalescent processes, two or more smaller droplets fuse to form one larger droplet. The chemistode relies on surface-induced coalescence<sup>11</sup> in a confined geometry. Here, we used a hydrophilic glass surface as the model substrate in the chemistode. The incoming plugs were flowing toward the hydrophilic surface at a constant velocity. The hydrophilic surface always held a wetting layer above the surface, until the incoming plug coalesced with the wetting layer and mass transfer occurred. When the response plugs re-formed, most of the original wetting layer had been replaced by the content of the incoming plug.

(2) Song, H.; Chen, D. L.; Ismagilov, R. F. *Angew. Chem., Int. Ed.* **2006**, *45*(44), 7336–7356.

(3) Priest, C.; Herminghaus, S.; Seemann, R. *Appl. Phys. Lett.* **2006**, *89*(13), 134101.

(4) Ahn, K.; Agresti, J.; Chong, H.; Marquez, M.; Weitz, D. A. *Appl. Phys. Lett.* **2006**, *88*(26), 264105.

(5) Kralj, J. G.; Schmidt, M. A.; Jensen, K. F. *Lab Chip* **2005**, *5*(5), 531–535.

(6) Baroud, C. N.; de Saint Vincent, M. R.; Delville, J. P. *Lab Chip* **2007**, *7*(8), 1029–1033.

(7) Song, H.; Tice, J. D.; Ismagilov, R. F. *Angew. Chem., Int. Ed.* **2003**, *42*(7), 768–772.

(8) Bremond, N.; Thiam, A. R.; Bibette, J. *Phys. Rev. Lett.* **2008**, *1*(2), 024501.

(9) Liu, K.; Ding, H. J.; Chen, Y.; Zhao, X. Z. *Microfluidics and Nanofluidics* **2007**, *3*(2), 239–243. Droplet-based synthetic method using microflow focusing and droplet fusion.

(10) Tan, Y. C.; Ho, Y. L.; Lee, A. P. *Microfluid. Nanofluid.* **2007**, *3*(4), 495–499.

(11) Fidalgo, L. M.; Abell, C.; Huck, W. T. S. *Lab Chip* **2007**, *7*(8), 984–986.

(12) Lorenz, R. M.; Edgar, J. S.; Jeffries, G. D. M.; Zhao, Y. Q.; McGloin, D.; Chiu, D. T. *Anal. Chem.* **2007**, *79*(1), 224–228.

\* To whom correspondence should be addressed. E-mail: r-ismagilov@uchicago.edu.

<sup>†</sup> The University of Chicago.

<sup>‡</sup> Current address: Department of Chemical Engineering, University of Illinois at Chicago, 810 S. Clinton Street, Chicago, IL 60607.

(1) Chen, D.; Du, W.; Liu, Y.; Liu, W.; Kuznetsov, A.; Mendez, F. E.; Philipson, L. H.; Ismagilov, R. F. *Proc. Natl. Acad. Sci. U.S.A.* **2008**, *105*, 16843–16848.

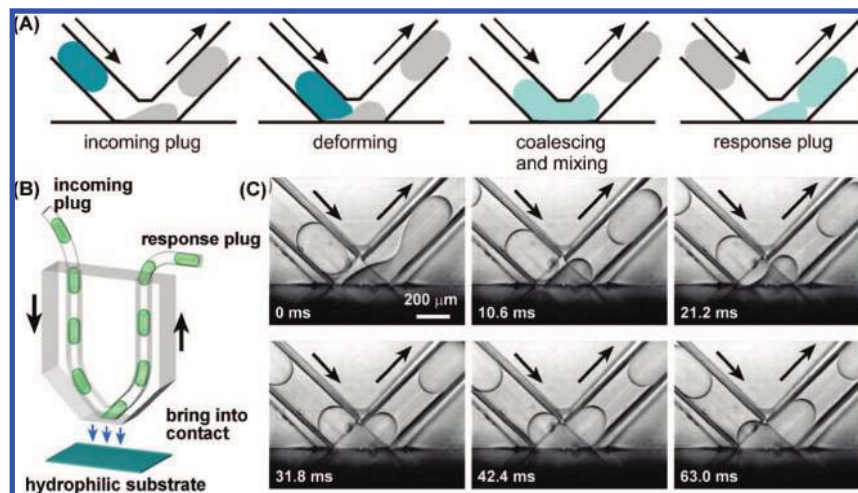


**Figure 1.** Process of incoming, deforming, coalescing and mixing, and re-forming of plugs in the chemistode. (A) Schematic drawing of incoming plug; deformation of the interface between the incoming plug and the wetting layer; coalescence and mixing of the plug and the wetting layer; and re-formation of the response plug. (B) Schematic drawing of the chemistode contacting a hydrophilic solid surface. (C) Time-lapse bright field images (side view) of an incoming plug merging with the wetting layer above a hydrophilic glass surface and re-formation of a response plug as the fluid exited.

Coalescence of the approaching plug and the wetting layer was necessary to ensure efficient mass transfer and to obtain high temporal resolution of stimulation and sampling. Although the energy barrier for coalescence in the absence of surfactant is reduced, surfactant such as triethyleneglycol mono[1H,1H-perfluorooctyl]ether (RfOEG) is required to make the system biocompatible and prevent adsorption of proteins to the aqueous–fluorous interface. It has been shown that RfOEG prevents nonspecific adsorption of proteins at the aqueous–fluorous interface in plug-based microfluidic systems.<sup>13</sup> Therefore, it is important to understand the dynamics of the coalescence in the chemistode to balance the mutually contradicting requirements of high time resolution and rapid coalescence, requiring low concentrations of surfactants, and compatibility with proteins, requiring high concentrations of surfactants.

The physics of coalescence of an individual plug with the wetting layer on the hydrophilic surface is interesting beyond applications of the chemistode for the following reasons. First, in this experiment, coalescence occurred in a microfluidic device with a fixed geometry. The hydrodynamic approach had a well-defined trajectory, and plug coalescence and re-formation was highly repeatable and reliable. The majority of current experimental studies on drop coalescence have involved measurements of the evolution of the size and size distribution of a dispersion system.<sup>14–16</sup> Although models based on average collision–coalescence probabilities have been developed to predict the final size distribution of the dispersion system,<sup>16</sup> and studies often show plausible agreement between experiments and models, it is especially interesting to be able to observe and understand coalescence of individual droplets.

Second, in this study, coalescence was induced by external flow. In the chemistode, while the wetting layer was held by the hydrophilic substrate, the incoming plug moved toward the wetting layer at constant velocity, until a significant amount of kinetic energy was converted to deformation energy, and then

the velocity of the incoming plug decreased. If the incoming plug failed to coalesce with the wetting layer, then the force decreased again as the plug left the hydrophilic substrate. Recently, theoretical studies have focused on numerical simulation of the interactions of two equal-sized spherical drops in a flow or in buoyancy driven motion, with or without surfactant, considering van der Waals forces or not.<sup>17–21</sup> These studies have made progress toward understanding the effects of external flow, surfactant, and viscosity ratio on the process of drainage of the film of carrier fluid. Although many theoretical studies have focused on the local deformation and formation of dimple regions,<sup>22</sup> it was found that the local deformation is not sufficient; rather, the overall deformation plays a key role.<sup>23</sup> Despite the theoretical study of flow induced coalescence, direct experimental observation and quantitative analysis remains challenging. The experimental study of coalescence of droplets in the microfluidic chemistode clarifies the dynamics of coalescence of individual droplets induced by an external flow field. Third, coalescence of incoming drops with drops located on solid substrates is not fully understood. During the free spreading of drops on a hydrophilic substrate, the bridge length scales with time,  $t$ , as  $t^{1/2}$ .<sup>24</sup> This simple scaling law does not apply to the confined geometry and external flow in our study, and the chemistode presented a more complicated problem.

In this Article, the effects on coalescence of droplets of (i) the velocity of the incoming plug, (ii) the viscosity ratio of the aqueous phase with the phase of fluorocarbon carrier fluid, and the (iii) surface tension between the aqueous and fluorocarbon phases were investigated. Uniquely, coalescence occurred in a microfluidic device that allowed the trajectory, deformation, coalescence, and re-formation of the drops to be highly reproducible.

(17) Yoon, Y.; Borrell, M.; Park, C. C.; Leal, L. G. *J. Fluid Mech.* **2005**, *525*, 355–379.

(18) Klaseboer, E.; Chevaillier, J. P.; Gourdon, C.; Masbernat, O. *J. Colloid Interface Sci.* **2000**, *229*(1), 274–285.

(19) Rekvig, L.; Frenkel, D. *J. Chem. Phys.* **2007**, *127*(13), 134701.

(20) Yeo, L. Y.; Matar, O. K.; de Ortiz, E. S. P.; Hewitt, G. F. *J. Colloid Interface Sci.* **2001**, *241*(1), 233–247.

(21) Yeo, L. Y.; Matar, O. K.; de Ortiz, E. S. P.; Hewitt, G. E. *J. Colloid Interface Sci.* **2003**, *257*(1), 93–107.

(22) Rother, M. A.; Davis, R. H. *Phys. Fluids* **2001**, *13*(5), 1178–1190.

(23) Baldessari, F.; Leal, L. G. *Phys. Fluids* **2006**, *18*(1), 013602.

(24) Ristenpart, W. D.; McCalla, P. M.; Roy, R. V.; Stone, H. A. *Phys. Rev. Lett.* **2006**, *97*(6), 064501.

(13) Roach, L. S.; Song, H.; Ismagilov, R. F. *Anal. Chem.* **2005**, *77*(3), 785–796.

(14) Bibette, J.; Morse, D. C.; Witten, T. A.; Weitz, D. A. *Phys. Rev. Lett.* **1992**, *69*(16), 2439–2442.

(15) Deminiere, B.; Colin, A.; Leal-Calderon, F.; Muzy, J. F.; Bibette, J. *Phys. Rev. Lett.* **1999**, *82*(1), 229–232.

(16) Burkhart, B. E.; Gopalkrishnan, P. V.; Hudson, S. D.; Jamieson, A. M.; Rother, M. A.; Davis, R. H. *Phys. Rev. Lett.* **2001**, *87*(9), 098304.

## Experimental Section

**Materials.** Unless otherwise stated, all chemicals were purchased at standard grades and used as received. Poly(ethylene glycol) (MW 3350) (PEG 3350) aqueous solution (50 wt %) was purchased from Hampton Research (Aliso Viejo, CA). In the experiments, 50 wt % PEG 3350 was diluted using MilliQ water to 20 wt %. The 20 wt % PEG 3350 aqueous solution has a dynamic viscosity of 9.5 mPa·s at room temperature and is a Newtonian fluid.<sup>25</sup> Fluorocarbon FC3283 and FC70 were purchased from 3M (St. Paul, MN). FC3283 was purified by distillation. Dynamic viscosities of FC3283 and FC70 at room temperature are 1.4 mPa·s and 27.2 mPa·s, respectively. Densities of FC3283 and FC70 at room temperature are 1.82 g·cm<sup>-3</sup> and 1.94 g·cm<sup>-3</sup>, respectively. Poly(tetrafluoroethylene) (PTFE) tubing was purchased from Zeus Industrial Products (Orangeburg, SCA) and introduced into PDMS microfluidic devices as described previously.<sup>26</sup> RfOEG was prepared according to published procedures.<sup>13</sup>

**Fabrication of Microfluidic Devices.** The chemistode consisted of V-shaped (90° angle) channels (square cross section of 300 μm × 300 μm) (Figure 1B). The device was fabricated by rapid prototyping soft lithography in poly(dimethylsiloxane) (PDMS).<sup>27</sup> The surfaces of the PDMS microchannels were made hydrophobic and fluorophilic by functionalization with (tridecafluoro-1,1,2,2-tetrahydrooctyl)-1-trichlorosilane.<sup>27</sup> PTFE tubing (200 μm I.D., 250 μm O.D.) was inserted into the square channels for the final construction of the chemistode. The gap between the PTFE tubing and the PDMS square channels of the device was sealed with PDMS. A T-shaped PDMS microfluidic device with square channels (cross section of 100 μm × 100 μm) was also fabricated by the above method for the purpose of generating plugs. The chemistode and the T-shaped device were connected by the PTFE tubing to allow the plugs generated in T-shaped device to flow into the chemistode.

**Surface Tension Measurements.** Surface tension was measured by the pendant drop method at room temperature using a Rame-Hart DROPimage (Rame-Hart instrument Co., Netcong, NJ) instrument. Equilibrium was reached within 40 s.

**Experimental Procedures.** Four concentrations of RfOEG in carrier fluid, FC3283 or FC70, were prepared: 0.25, 0.5, 0.75, and 1 mg·mL<sup>-1</sup>. The critical micelle concentration (CMC) of RfOEG in FC3283 is higher than 1 mg/mL. Measured by NMR, the CMC was not found for concentrations of surfactant up to 1 mg/mL.<sup>13</sup> All the plugs were generated at a constant capillary number,  $Ca = 3 \times 10^{-4}$ , in the T-shaped microfluidic device. The plugs were delivered to the chemistode by using syringe pumps (PHD2000, Harvard Apparatus, Holliston, MA). All the plugs had similar size ( $l \approx 2.5d$ , where  $l$  is the plug length and  $d = 200 \mu\text{m}$  is the tubing diameter). The open end of the chemistode was pressed against a glass slide, which was plasma oxidized for 100 s. Images were taken by using an inverted microscope (Leica IRE2, Wetzlar, Germany) equipped with a high speed Phantom 7.1 camera (Vision Research, Stuart, FL) at 4700 fps.

## Results and Discussion

**Coalescence in the Chemistode.** In this study, the description of coalescence (Figure 1) required four independent dimensionless parameters,

$$\tau = t_{\text{coalescence}} \omega = \frac{t_{\text{coalescence}}}{L/(\phi U)}, \quad Ca = \frac{\mu_f U}{\sigma}, \quad \lambda = \frac{\mu_a}{\mu_f},$$

$$\text{and } Pe = \frac{U_f \delta_0}{D_s} \quad (1)$$

Here,  $\tau$  defines the nondimensional coalescence time, which is the ratio of coalescence time  $t_{\text{coalescence}}$  (s) over the time required

for two consecutive plugs to pass over the same point in the chemistode.  $t_{\text{coalescence}}$  (s) is the coalescence time, which is defined here as the sum of the drainage time and rupture time. The drainage time starts when the incoming plug is sufficiently close to the wetting layer to induce deformation of their interface. The rupture time begins when the incoming plug starts to coalesce (film ruptures) with the wetting layer and lasts until the interface becomes smooth.  $\omega$  (s<sup>-1</sup>) is the frequency with which incoming plugs arrive.  $L$  (m) is the plug length.  $U$  (m·s<sup>-1</sup>) is the average flow velocity.  $\phi$  is the water fraction,<sup>28</sup> which was 0.5 for all the conditions described in this paper.  $Ca$  is the capillary number, which defines the ratio of viscous energy over surface energy.  $\mu_f$  (kg·m<sup>-1</sup>·s<sup>-1</sup>) is the viscosity of the fluorocarbon carrier fluid, and  $\sigma$  (N·m<sup>-1</sup>) is the surface tension between the aqueous and fluorocarbon phases.  $\lambda$  is the viscosity ratio of the aqueous phase, that is, the incoming plug and the wetting layer, over the fluorocarbon phase, that is, the carrier fluid.  $\mu_a$  (kg·m<sup>-1</sup>·s<sup>-1</sup>) is the viscosity of the aqueous phase.  $Pe$  is the Peclet number for the surfactant, which compares the rate of surfactant transport by convection and by diffusion.  $U_f$  (m·s<sup>-1</sup>) is the tangential velocity of the carrier fluid between the incoming plug and the wetting layer, and  $D_s$  (m<sup>2</sup>·s<sup>-1</sup>) is the surface diffusivity of the surfactant, RfOEG, at the interface of the incoming plug and the wetting layer. The value of  $D_s$  should be between O (10<sup>-11</sup> m<sup>2</sup>·s<sup>-1</sup>)<sup>29</sup> and O (10<sup>-9</sup> m<sup>2</sup>·s<sup>-1</sup>).<sup>30</sup> As a rough estimate, the surface diffusivity of RfOEG was taken as 10<sup>-10</sup> m<sup>2</sup>·s<sup>-1</sup>.  $\delta_0$  is the thickness of the film, which is estimated as 1 μm right before film rupture starts.

The process of coalescence and re-forming of plugs consisted of four stages (Figure 1A). In the first stage, the incoming plug flowed toward the surface. This stage is controlled by the hydrodynamic flow velocity, which was kept constant in our experiments. The second stage was the drainage of the thin film of carrier fluid. During this stage, the kinetic energy was converted to deformation energy, and the velocity of the incoming plug was lower than that in the first stage. The third stage occurred when the distance between the incoming plug and the wetting layer became small enough that nonhydrodynamic attractive forces (i.e., van de Waals forces) induced instability and the film ruptured. In the absence of surfactant, the thin film is thermodynamically unstable, and film rupture can be faster than microseconds. Here, we used RfOEG, which prevents adsorption of protein at the interface, as the surfactant. The presence of surfactant prolongs the time for film rupture because of higher free energy barrier and kinetics of surfactant adsorption–desorption. Although the time for film rupture was prolonged by adding surfactant, this time remained much shorter than the time for drainage of carrier fluid, as observed in the experiments. The fourth stage was re-forming of the response plug when surface tension cannot balance the viscous force.

**Effect of Capillary Number ( $Ca$ ).** We found that the coalescence time,  $\tau$ , was a function of the capillary number,  $Ca$  (Figure 2A). At a constant capillary number, the coalescence time,  $\tau$ , did not change as we varied either surface tension or velocity of the incoming plug. In other words, neither surface tension alone nor velocity alone are sufficient to describe  $\tau$ , whereas  $Ca$  alone does describe  $\tau$ . Two regimes have been observed in these experiments (Figure 2A). We refer to these regimes as (I) rupture starting at the nose region and (II) rupture

(25) Gonzalezteello, P.; Camacho, F.; Blazquez, G. *J. Chem. Eng. Data* **1994**, 39(3), 611–614.

(26) Li, L.; Mustafi, D.; Fu, Q.; Tereshko, V.; Chen, D. L. L.; Tice, J. D.; Ismagilov, R. F. *Proc. Natl. Acad. Sci. U.S.A.* **2006**, 103(51), 19243–19248.

(27) Duffy, D. C.; McDonald, J. C.; Schueller, O. J. A.; Whitesides, G. M. *Anal. Chem.* **1998**, 70(23), 4974–4984.

(28) Tice, J. D.; Song, H.; Lyon, A. D.; Ismagilov, R. F. *Langmuir* **2003**, 19(22), 9127–9133.

(29) Agrawal, M. L.; Neuman, R. D. *J. Colloid Interface Sci.* **1988**, 121(2), 366–380.

(30) Miller, R.; Li, J. B.; Bree, M.; Loglio, G.; Neumann, A. W.; Mohwald, H. *Thin Solid Films* **1998**, 327, 224–227.

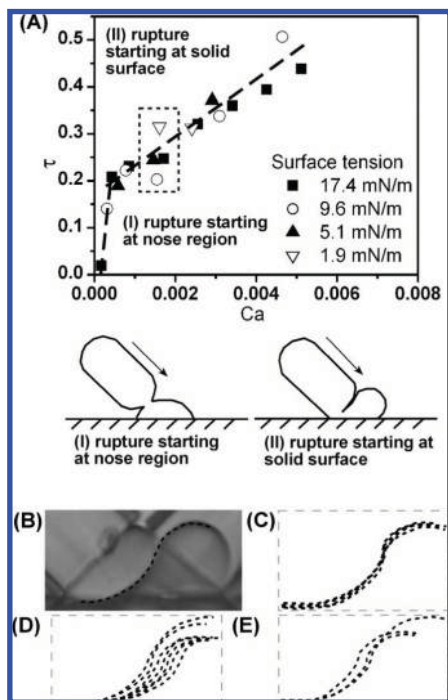


**Figure 2.** Coalescence time depends on capillary number. (A) Non-dimensional coalescence time,  $\tau$ , is a function of capillary number,  $Ca$ , at various surface tensions. Two coalescence regimes are observed: (I) coalescence starting at the nose region and (II) coalescence starting at the hydrophilic surface. (B and C) Example of overall deformation of plugs at  $Ca = (1.6 \pm 0.1) \times 10^{-3}$  and different surface tensions and flow velocities immediately prior to film rupture (cases circled by the gray dashed line in Figure 2A). (B) Bright field image of the deformation immediately before film rupture started. The dashed line is the contour of the deformed interface of the incoming plug and the wetting layer. (C) Overlaps of the contours indicate similar overall deformation at different surface tensions but with similar  $Ca$ . (D) Profiles of the interface between the incoming plug and the wetting layer prior to film rupture. Surface tension was 17.4 mN/m. Velocities varied from 5.3 to 63.7 mm/s. (E) Profiles of the interface between the incoming plug and the wetting layer prior to film rupture. Velocity of the incoming plug was 5.3 mm/s. Surface tensions were 17.4, 9.6, and 5.1 mN/m.

starting at the solid surface. In each regime, the relationship between  $\tau$  and  $Ca$  was an approximately linear function. Thus, the resulting type of regime depended on  $Ca$ . In regime I, the incoming plug flowed in at very low  $Ca$  ( $Ca < 3 \times 10^{-4}$ ) (Figure 2A). Thinning of the film occurred rapidly, and rupture of the film occurred in the nose region, before any significant deformation of the interface could occur, because, at low  $Ca$ , the hydrodynamic force was insufficient for deformation. As  $Ca$  increased, deformation began to be obvious, and the coalescence time increased. In regime II, the film rupture always started at the hydrophilic surface and then propagated away from the hydrophilic surface (Figure 2A). Furthermore,  $Ca$ , instead of approach velocity or surface tension alone, defined the overall deformation of the plugs just before film rupture occurred. We observed similar shapes of deformation profiles, measured just before film rupture, under four conditions characterized by the same  $Ca$  but with different surface tensions and flow velocities (Figure 2B and C). When we kept constant surface tensions (Figure 2D) or flow velocities (Figure 2E) instead of  $Ca$ , we observed that the deformation profiles prior to film rupture were different. This result, that the overall deformation instead of the local deformation within the film plays the key role in determining the coalescence efficiency, was consistent with the previous results of numerical simulations<sup>23</sup> of the collision and coalescence of two equal-sized spherical drops introduced by a flow field.

**Critical Capillary Number ( $Ca_c$ ).** We observed that, for higher  $Ca$ , the coalescence time was longer. We also found a critical capillary number,  $Ca_c$ , such that, for a  $Ca$  below the critical value, coalescence occurred between the incoming plug and the wetting layer on the hydrophilic substrate, whereas, for a  $Ca$  above the critical value, the incoming plug passed by the substrate without coalescence (Figure 3A).  $Ca_c$  was an increasing function of surface tension (Figure 3B) and was independent of viscosity ratio (Figure 3C).

We attribute the dependence of  $Ca_c$  on surface tension,  $\sigma$ , to dynamics of assembly and transport of surfactant. In these experiments, the bulk surfactant concentration,  $C$  ( $\text{mg} \cdot \text{mL}^{-1}$ ), varied from 0.25 to 1  $\text{mg} \cdot \text{mL}^{-1}$ , and  $\sigma$  and  $\ln(C)$  were linearly related (Figure 4). Because R/OEG does not have a distinct critical micelle concentration in FC3283, the curve did not reach the plateau at high concentration. Surface excess of the surfactant at equilibrium,  $\Gamma$  ( $\text{mol} \cdot \text{m}^{-2}$ ), estimated by using the Gibbs equation for the nonionic surfactant system,<sup>31</sup>  $\Gamma = (-1/RT)(d\sigma/d \ln(C))$ , was constant. For stable surfactants with constant density, the above equation is valid for the concentration of the surfactant  $C$  expressed in any units, since  $d \ln(C) = (1/C)dC$  is nondimensional. In other words, regardless of the units used to express  $C$ ,  $d \ln(C)$  can be rewritten as  $(1/C)dC$ , and in this expression units of  $C$  cancel; therefore, the value of  $d \ln(C)$  will not depend on the units used to express  $C$ . Here, we analyzed the surface excess of the surfactant (R/OEG) by plotting surface tension and  $\ln(C)$  for surfactant concentration in terms of  $\text{mg} \cdot \text{mL}^{-1}$ .  $R$  ( $\text{J} \cdot \text{K}^{-1} \cdot \text{mol}^{-1}$ ) is the gas constant and  $T$  (K) is the Kelvin temperature. Therefore, dependence of  $Ca_c$  on surface tension is not a result of differential coverage of the surface by the surfactant. We attribute this dependence of  $Ca_c$  on surface tension to the difference in time required for surfactant to reach the equilibrium coverage under conditions of different surface tensions and different concentrations. Surface tension measurements we have performed correspond to equilibrium surface tensions, attained on the time scale of tens of seconds. The events we are measuring take place on the millisecond time scale, and therefore, they do not provide enough time to reach these equilibrium surface tensions. Further studies to measure dynamic surface tensions on millisecond time scales in this system would be valuable.

The deformation stretched the interface, decreasing to below the equilibrium value the local surface coverage by the surfactant at the interface. At low velocity regimes, diffusion could be comparable with convection. For most operation conditions we are interested in, we used  $Pe > 1$  as an estimation. The typical Peclet number in all the experimental cases was  $O(10^1 - 10^3)$ , considering  $U \sim O(10^{-3} - 10^{-1} \text{ m} \cdot \text{s}^{-1})$ ,  $\delta_0 = 1 \mu\text{m}$ , and  $D_s \sim 10^{-10} \text{ m}^2 \cdot \text{s}^{-1}$  as discussed in the previous section. Therefore, surface extension induced by the flow field was faster than surfactant surface diffusion. At higher bulk concentration of the surfactant, although the equilibrium surface coverage was constant, the surfactant recovered more quickly from the reduced concentration of surfactant at the local interface and reached equilibrium faster, preventing coalescence from occurring. Therefore, from the point view of surfactant dynamics, at higher surfactant concentration,  $Ca_c$  was lower and the coalescence region was smaller.

Coalescence time did not depend on the viscosity of the aqueous phase (data not shown), and the viscosity of the carrier fluid was included in the definition of  $Ca$  (see above). Because  $Ca_c$  was independent of the viscosity of the carrier fluid as

(31) Adamson, A. W.; Gast, A. P. *Physical Chemistry of Surfaces*, 6th ed.; John Wiley and Sons, Inc.: New York, 1997; pp 80–92.

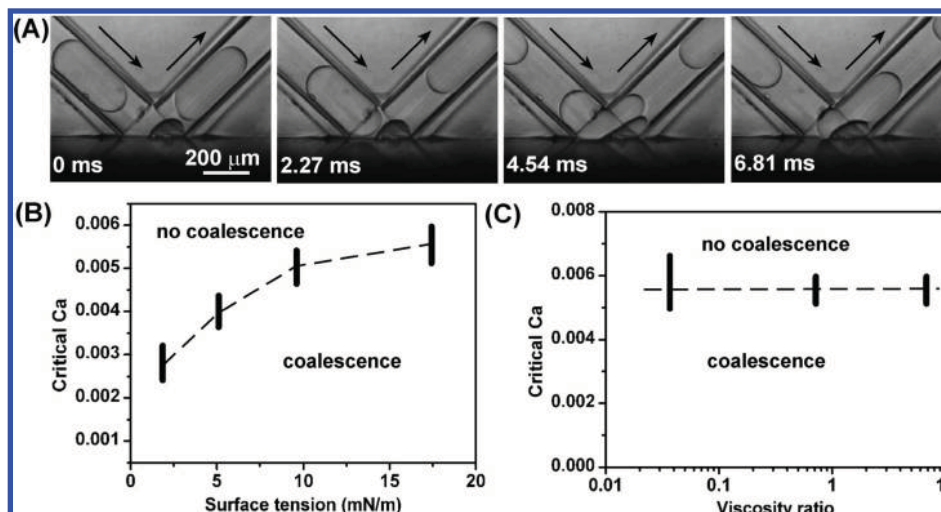


**Figure 3.** Critical capillary number ( $Ca_c$ ) defines the limit of coalescence, and it depends on surface tension but not viscosity ratio. (A) Time-lapse bright field images (side view) of the approaching plug passing by the wetting layer without coalescence. The surface tension was  $9.6 \text{ mN}\cdot\text{m}^{-1}$ , and the  $Ca$  was 0.006. (B) Plot of critical capillary number ( $Ca_c$ ) as a function of surface tension ( $\sigma$ ). Symbols indicate the range of  $Ca_c$  within which the transition from coalescence to no coalescence occurs. (C) Plot of  $Ca_c$  as a function of viscosity ratio. In experiments in (B) and (C), the velocity was changed in discrete steps rather than continuously, and therefore, only the range, rather than the exact transition point, could be identified.

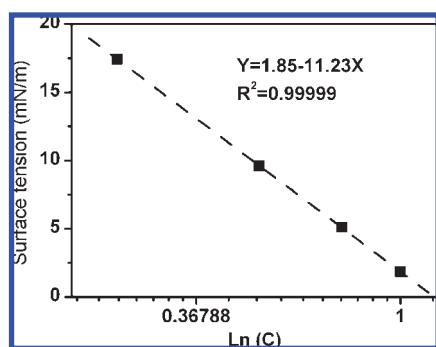


**Figure 4.** Surface tension,  $\sigma$ , as a function of the natural logarithm of surfactant concentration,  $\ln(C)$ . The linear relationship of surface tension with  $\ln(C)$  indicated that at equilibrium the surface coverage was saturated for all of these concentrations. The conclusions are not dependent on the units used, because  $d \ln(C) = (1/C)dC$  is nondimensional. In this figure, values of  $C$  were used with units of mg/mL. In these experiments, the surfactant was RfOEG and the carrier fluid was FC3283.

well as the viscosities of the plug and wetting layer,  $Ca_c$  was therefore independent of the viscosity ratio of the two phases (Figure 3B). The limit of the temporal resolution for systems with different viscosities of carrier fluid could be estimated by  $t_{\min} \sim L/(\phi U_{\max}) = (L/\phi)(\mu_f/Ca_c\sigma)$ . For RfOEG as the surfactant,  $0.5 \text{ mg}\cdot\text{mL}^{-1}$  concentration is typically used to prevent adsorption of proteins at the interface. At this concentration of RfOEG, the surface tension is  $9.6 \text{ mN}\cdot\text{s}^{-1}$  and  $Ca_c$  is 0.0054, which limited the frequency of plugs passing by the surface to 50 plugs per second using FC3283 as the carrier fluid and 3 plugs per second using FC70 as the carrier fluid.

**Film Rupture.** Film rupture was the last step of coalescence. In the chemistode in regime II (Figure 2), we observed a unique phenomenon: rupture starting at the hydrophilic surface. This mode of rupture presumably was responsible for the observed repeatable and reliable pattern of coalescence. At  $3 \times 10^{-4} < Ca < Ca_c$ , the coalescence started from the interface of the incoming plug and the hydrophilic surface. As the fluorocarbon carrier fluid was continuously drained out, film rupture propagated away from the surface until the interface between the plug and

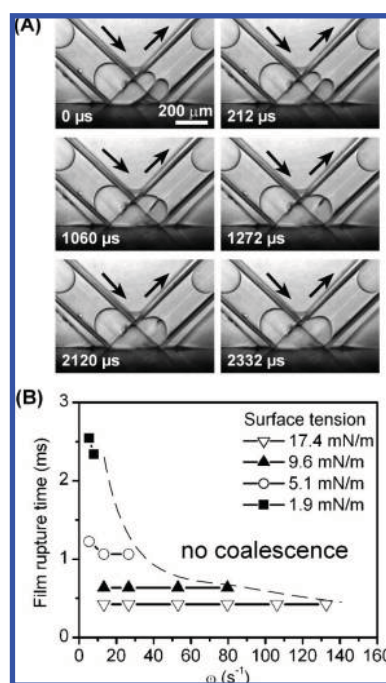


**Figure 5.** Images of film rupture (regime II). Time for film rupture inversely depends on surface tension. (A) Series of time-lapse bright field images of type II (coalescence starting at the hydrophilic surface) film rupture at  $Ca = 1.6 \times 10^{-3}$  and  $\sigma = 1.85 \text{ mN}\cdot\text{m}^{-1}$ . (B) Rupture time plotted as a function of the frequency of incoming plugs at various surface tensions.

the wetting layer became smooth (Figure 5A). Film rupture time was inversely dependent on surface tension (Figure 5B). With the increase of bulk surfactant concentration, surface tension decreases, and the time for rupture of the thin film increases, presumably due to the slower desorption of surfactant from the interface into the carrier fluid. Only at high surfactant concentrations does the film rupture time weakly depend on the frequency (and, therefore, velocity) of incoming plugs. At high surfactant concentrations, the film rupture time is prolonged and therefore plug kinetics affect film rupture (Figure 5B).

## Conclusions

We have presented an investigation of the coalescence of droplets in a microfluidic device with fixed geometry. The coalescence of an incoming plug with a wetting layer was highly repeatable and reliable. In contrast to most studies on droplet coalescence, which have focused on the coalescence probability, emulsion stability, and mean droplet size,<sup>14–16</sup> here we observed coalescence of individual droplets. Uniquely, plugs were constantly re-formed after mass transfer between the wetting layer and the incoming, resulting in a same-sized response plugs for further analysis. Reliable coalescence is essential for the chemistode to be applied in chemical and biological stimulation and recording.

These results show that the trajectory analysis used to determine the effects of small deformations on the coalescence efficiency of two moving drops in a linear flow at small capillary number does not apply to the chemistode. This result is not surprising given the presence of the hydrophilic surface. The experimental results further showed that coalescence within the chemistode pressed against the hydrophilic surface depended only on capillary number. In the regime II, where the film rupture started at the surface, the coalescence time was a linear function of  $Ca$ . Of course, correlation is not causation, and just because we see that  $Ca$  is a good descriptor of the phenomenon, it does not mean it is the best or the most physically relevant, and alternative descriptors should be tested in future work. The critical capillary number defined the boundary between regimes of coalescence

and noncoalescence. This critical capillary number was determined by the concentrations of surfactant and, presumably, by the rate of assembly of the surfactant at the interface and by the molecular structures of the surfactant. With a given surfactant, the critical capillary number was higher at a lower surfactant concentration. Neither the viscosity of the carrier fluid nor the viscosity of the aqueous phase affected the critical capillary number. In this study, only a chemistode with 90° V-shaped channels was discussed. The additional effects of geometry, as well as of other surfactant molecules, will need to be addressed in future studies. It also remains to be seen whether these findings describe coalescence in other systems described previously<sup>8,11</sup> and in systems designed for injection of reagents into plugs via hydrophilic channels.<sup>2,32,33</sup>

**Acknowledgment.** This work was supported by NSF Materials Research Science and Engineering Center Grant 0213745. R.F.I. is a Cottrell Scholar of Research Corporation and a Camille Dreyfus Teacher-Scholar. Part of this work was performed at the Chicago MRSEC. We thank Sidney R. Nagel and Wendy Zhang for helpful discussion, Jason E. Kreutz for synthesizing RfOEG, Wenbin Du for help with the chemistode fabrication, and Elizabeth W. Boyd for contributions to editing this manuscript.

LA803518B

(32) Zheng, B.; Ismagilov, R. F. *Angew. Chem., Int. Ed.* **2005**, *44*(17), 2520–2523.

(33) Li, L.; Boedicker, J. Q.; Ismagilov, R. F. *Anal. Chem.* **2007**, *79*(7), 2756–2761.